Spectral features of polaronic excitations in a superconducting analog simulator

Julian K. Nauth and Vladimir M. Stojanović
Institut für Angewandte Physik, Technical University of Darmstadt, D-64289 Darmstadt, Germany

(Received 26 January 2023; accepted 3 May 2023; published 17 May 2023)

We investigate the spectral properties of polaronic excitations within the framework of an analog quantum simulator based on inductively coupled superconducting transmon qubits and microwave resonators. This system emulates a lattice model that describes a nonlocal coupling of an itinerant spinless-fermion excitation to dispersionless (Einstein-type) phonons through the Peierls and breathing-mode interaction mechanisms. The model is characterized by a sharp, level-crossing transition at a critical value of the effective excitation-phonon coupling strength; above the transition point, the ground state of this model corresponds to a heavily dressed (small-polaron) excitation. Using the kernel-polynomial method, we evaluate the momentum-frequency resolved spectral function of this system for a broad range of parameters. In particular, we underscore the ramifications of the fact that the zero-quasimomentum Bloch state of a bare excitation represents the exact eigenstate of the Hamiltonian of this system for an arbitrary excitation-phonon coupling strength. We also show that—based on the numerically evaluated spectral function and its well-known relation with the survival probability of the initial, bare-excitation Bloch state (the Loschmidt echo)—one can make predictions about the system dynamics following an excitation-phonon interaction quench. To make contact with anticipated experimental realizations, we utilize a previously proposed method for extracting dynamical-response functions in systems with local (single-qubit) addressability using the multiqubit (many-body) version of the Ramsey interference protocol.

DOI: 10.1103/PhysRevB.107.174306

I. INTRODUCTION

The field of quantum simulation [1] rose to prominence over the past decade as a thriving research area at the intersection of the traditional fields of condensed-matter physics and atomic, molecular, and optical physics, on the one hand, and the rapidly developing field of quantum information processing on the other. In particular, analog quantum simulators provide valuable insights into various properties of complex many-body systems [2–8], while at the same time typically requiring much more modest quantum-hardware resources—i.e., a smaller number of qubits—for their realization than what will eventually be required for large-scale universal quantum computation. Examples of physical platforms usually employed for implementing analog quantum simulators are furnished by those based on cold neutral atoms in optical lattices [9] or tweezers [10], trapped ions [11], cold polar molecules [12], and superconducting (SC) quantum circuits [13,14]. The latter usually entail transmon qubits [15] and SC microwave resonators, the key building blocks of circuit quantum electrodynamics (circuit-QED) systems [16–18]; analog simulators with similar functionalities can also be realized with flux qubits [19,20].

Analog simulators of quantum many-body systems are typically designed with the aim of investigating their ground-state (static) or dynamical properties [1]. On the other hand, it was only recently that some attention was also dedicated to elucidating *spectral properties* of such systems by virtue of analog simulators [21,22]. Motivated in part by the apparent dearth of studies pertaining to this important aspect of simulated many-body systems, the present work is devoted to spectral properties of a one-dimensional system that comprises an itinerant spinless-fermion excitation coupled to dispersionless (zero-dimensional) phonons through two nonlocal coupling mechanisms—more precisely, Peierls- and breathing-mode type excitation-phonon (e-ph) interactions [23,24]. The present study is framed within the context of an analog SC quantum simulator, which was previously proposed for studying both static [23] and dynamical [24] properties of this coupled e-ph system. The principal building blocks of this simulator are transmon qubits and microwave resonators [14,25–28]. Importantly, the qubit-resonator coupling in this simulator belongs to the class of indirect inductive couplings [29], and the physical mechanism that enables it entails a flux of the resonator (microwave-photon) modes that pierces specially tailored coupler circuits connecting adjacent qubits. In this system, SC qubits are coupled through nearest-neighbor XY-type (flip-flop) interaction whose effective strength depends dynamically on the resonator degrees of freedom (i.e., photons), this dependence being equivalent to that of the XY spin-Peierls model [30,31].

The quantity of primary interest in our present context is the *momentum-frequency resolved spectral function*, this last dynamical response function being closely related to the Fourier transform of the single-particle retarded Green's function [32]. This spectral function, which captures *inter alia* the essential features of dressed polaronic excitations in the strong-coupling regime of the system under consideration, will be evaluated here in a numerically exact manner. To be more specific, the *kernel-polynomial method* (KPM) [33]—based on the expansion of the relevant spectral function in Chebyshev polynomials of the first kind—will be utilized here for computing the spectral function for various choices of parameters characterizing the SC analog simulator under

consideration. The KPM, pioneered by Silver and Röder [34], was successfully employed in the past for evaluating both zero- [35] and finite-temperature [36] dynamical response functions in a variety of quantum many-body systems [33]. Motivated by the need to accurately compute spectral densities of strongly interacting quantum many-body systems, various generalizations of this method have also been proposed [37].

What makes the proposed analysis of momentum-frequency resolved spectral functions within the framework of a SC analog simulator particularly pertinent is the availability of a method for the experimental measurements of such quantities and their counterparts in the time domain [38]. This method is based on a generalized, multiqubit version of the Ramsey interference protocol [39] (recall that, when applied to a single SC qubit, the Ramsey interference protocol is used to determine its dephasing time T_2 [40]) and is applicable to all locally addressable systems [23]. In particular, being amenable to experimental control at the single-qubit level, the envisioned SC analog simulator constitutes a nearly ideal platform for the practical demonstration of this method.

Heavily dressed quasiparticles formed in the strong-coupling regime of systems that feature short-range interaction of an itinerant excitation (electron, hole, exciton) with dispersionless (Einstein-like) phonons are referred to as *small polarons*. While the Holstein model [41], describing local e-ph interaction [42–44], is the most common starting point for investigating such quasiparticles, more realistic models that involve nonlocal e-ph coupling mechanisms have come to the fore over the past decade. These mechanisms—exemplified by Peierls- [45] and breathing-mode-type [46] e-ph couplings—are known to play important roles in certain classes of narrowband electronic materials [47–56]. Moreover, models involving Peierls-type coupling show sharp, level-crossing transitions in the ground-state-related quantities at certain critical values of the effective e-ph coupling strength [57]; such couplings, whose corresponding e-ph vertex functions depend on both excitation and phonon quasimomenta, do not belong to the realm of validity of the time-honored Gerlach-Löwen theorem [58] that rules out such nonanalyticities for most known e-ph interaction types. Finally, those models also display nontrivial e-ph entanglement properties, both in the ground [57,59] and excited states [60].

Several analog simulators of the Holstein model have as yet been proposed that make use of physical platforms as diverse as trapped ions [61], cold polar molecules [62], and SC circuits [63]. On the other hand, models that involve nonlocal (momentum-dependent) e-ph interactions have as yet only been simulated using arrays of SC qubits and microwave resonators [23,24], where photons in resonators play the role of phonons. The previous studies covered both ground-state [23] and dynamical [24] properties of small polarons in such models, which motivates us to also investigate their spectral properties in the present work.

The outline of the remainder of this paper is as follows. In Sec. II the spectral properties of dressed excitations are briefly reviewed, starting with general features of momentum-frequency resolved spectral functions. This is followed by a brief summary of the Ramsey-protocol based method for extracting spectral functions experimentally in Sec. III. In Sec. IV, the analog simulator under consideration and its governing Hamiltonian are introduced, along with a brief description of the derivation of its effective Hamiltonian. The numerical results obtained for the momentum-frequency resolved spectral function of this system are presented and discussed in Sec. V. Finally, the paper is summarized, with some general concluding remarks, in Sec. VI. Some mathematical details pertaining to the form of the qubit-qubit interaction in the system at hand, the truncation of the Hilbert space of the system, and the use of the KPM for computing the spectral function are relegated to Appendixes A, B, and C, respectively.

II. MOMENTUM-FREQUENCY RESOLVED SPECTRAL FUNCTION

Dynamical response functions, defined through Fourier transforms of retarded two-time correlation functions, provide a framework for characterizing excitations in many-body systems and are intimately related to their resulting magnetic, optical, and transport properties [32]. Among the relevant two-time correlation functions, a particularly important example is furnished by the single-particle retarded Green's function, which conventionally describes the propagation of a single electron (or a hole). Here this Green's function will be employed in the context of an itinerant spinless-fermion excitation that interacts with zero-dimensional bosons residing on sites of a one-dimensional lattice.

The single-particle retarded Green's function of interest in the problem under consideration is given by

$$G_+^{\mathrm{R}}(k,t) = -\frac{i}{\hbar}\theta(t)\langle \mathrm{G}_0|[c_k^\dagger(t), c_k]_+|\mathrm{G}_0\rangle. \tag{1}$$

Here $c_k^\dagger(t) \equiv U_H^\dagger(t) c_k^\dagger U_H(t)$ is a single-particle creation operator in the Heisenberg representation, where $U_H(t)$ is the time-evolution operator of the system, with H being its governing Hamiltonian; $\theta(t)$ is the Heaviside step function, $|\mathrm{G}_0\rangle$ is the ground state of the system, and $[\cdots]_+$ denotes an anticommutator.

The last retarded Green's function describes the linear response of the system to the addition and removal of a single fermion. To formally evaluate its Fourier transform, a regularization factor $\lim_{\eta\to 0^+} e^{-\eta|t|}$ ought to be included. Accordingly, the regularized Fourier transform of $G_+^{\mathrm{R}}(k,t)$ is given by

$$G_+^{\mathrm{R}}(k,\omega) = \int_{-\infty}^{\infty} G_+^{\mathrm{R}}(k,t) e^{i\omega t - \eta|t|} dt \quad (\eta \to 0^+), \tag{2}$$

and—with the aid of Eq. (1)—leads to

$$G_+^{\mathrm{R}}(k,\omega) = \langle \mathrm{G}_0|c_k \frac{1}{\hbar\omega + i0^+ + E_0 - H} c_k^\dagger|\mathrm{G}_0\rangle + \langle \mathrm{G}_0|c_k^\dagger \frac{1}{\hbar\omega + i0^+ - E_0 + H} c_k|\mathrm{G}_0\rangle, \tag{3}$$

where E_0 is the ground-state energy of the system.

The quantity of primary interest for the present work, the *momentum-frequency resolved spectral function*, is given by

$$A(k,\omega) = -\frac{1}{\pi}\mathrm{Im}\, G_+^{\mathrm{R}}(k,\omega). \tag{4}$$

This single-particle spectral function can be expressed explicitly in terms of the eigenstates and eigenvalues of the Hamiltonian H, namely as

$$A(k,\omega) = \sum_j \left|\langle\psi_k^{(j)}|c_k^\dagger|0\rangle\right|^2 \delta\left(\omega - E_k^{(j)}/\hbar\right), \tag{5}$$

where $|\psi_k^{(j)}\rangle$ are the eigenstates and $E_k^{(j)}$ the corresponding eigenvalues of the Hamiltonian H with quasimomentum k. This spectral function satisfies the sum rule

$$\int_{-\infty}^{\infty} A(k,\omega)d\omega = 1 \tag{6}$$

for each quasimomentum k.

In the coupled e-ph system to be addressed in what follows, the last spectral function is intimately related to the system dynamics following an e-ph interaction quench. Namely, assuming the initial ($t = 0$) states to have the form of bare-excitation Bloch states $c_k^\dagger|0\rangle$ at different quasimomenta k (where $|0\rangle$ is the vacuum state of the system), the spectral function $A(k,\omega)$ is given by the Fourier transform of the matrix element $\langle\psi(t)|c_k^\dagger|0\rangle$ [where $|\psi(t)\rangle$ is the state of the system at time t]—the amplitude for the system to remain in the initial (bare-excitation) state at time t. This quantity represents the special case of what is more generally referred to as the Loschmidt amplitude, and its squared module (i.e., the survival probability of the initial state)

$$\mathcal{L}_k(t) \equiv |\langle\psi(t)|c_k^\dagger|0\rangle|^2 \tag{7}$$

is known as the Loschmidt echo [64]. The latter constitutes the most widely used quantity for characterizing nonequilibrium quantum dynamics [65].

III. MEASUREMENT OF THE RETARDED GREEN'S FUNCTION USING RAMSEY PROTOCOL

In the following, we first introduce the retarded single-particle Green's functions of relevance for the present work (Sec. III A). We then recapitulate the basics of the method for the experimental measurement of those Green's functions using a many-body (multiqubit) version of the Ramsey interference protocol (Sec. III B), which was proposed in Ref. [38] and adapted for application in systems of the kind discussed here in Ref. [23].

A. Retarded single-particle Green's functions

While the anticommutator Green's function [cf. Eq. (1)] is the appropriate one to use for spinless-fermion excitations in the problem under consideration, its commutator counterpart,

$$G_-^{\rm R}(k,t) = -\frac{i}{\hbar}\theta(t)\langle{\rm G}_0|[c_k^\dagger(t), c_k]_-|{\rm G}_0\rangle, \tag{8}$$

is essentially equivalent in the problem at hand. Because here $|{\rm G}_0\rangle = |0\rangle$ is the vacuum state of the coupled e-ph system, $c_k^\dagger(t)c_k|{\rm G}_0\rangle = 0$, implying that here $G_-^{\rm R}(k,t) = -G_+^{\rm R}(k,t)$.

The real-space retarded (commutator) Green's functions

$$G_{nn'}^{\rm R}(t) \equiv -\frac{i}{\hbar}\theta(t)\langle{\rm G}_0|[c_n^\dagger(t), c_{n'}]_-|{\rm G}_0\rangle, \tag{9}$$

which in systems with a discrete translational symmetry depend only on $n - n'$, are obtained from the above momentum-space ones [cf. Eq. (8)] via Fourier transformation:

$$G_-^{\rm R}(k,t) = N^{-1}\sum_{n,n'} e^{ik(n-n')}G_{nn'}^{\rm R}(t). \tag{10}$$

These real-space commutator Green's functions can be straightforwardly recast as [23]

$$G_{nn'}^{\rm R}(t) = -\frac{i}{\hbar}\theta(t)\langle{\rm G}_0|[\sigma_n^+(t), \sigma_{n'}^-]_-|{\rm G}_0\rangle, \tag{11}$$

where we have switched from spinless-fermion to the pseudospin-1/2 operators via the Jordan-Wigner (JW) transformation [66]:

$$\begin{aligned}\sigma_n^z &= 2c_n^\dagger c_n - 1,\\ \sigma_n^+ &= 2c_n^\dagger e^{i\pi\sum_{l<n}c_l^\dagger c_l}.\end{aligned} \tag{12}$$

These last Green's functions can succinctly be rewritten in the form [23]

$$G_{nn'}^{\rm R}(t) = \mathcal{G}_{nn'}^{xx} + \mathcal{G}_{nn'}^{yy} - i\left(\mathcal{G}_{nn'}^{xy} - \mathcal{G}_{nn'}^{yx}\right), \tag{13}$$

where $\mathcal{G}_{nn'}^{\alpha\beta}$ ($\alpha,\beta = x,y$) are retarded pseudospin correlation functions, defined as [23]

$$\mathcal{G}_{nn'}^{\alpha\beta} \equiv -\frac{i}{\hbar}\theta(t)\langle{\rm G}_0|\left[\sigma_n^\alpha(t), \sigma_{n'}^\beta\right]_-|{\rm G}_0\rangle. \tag{14}$$

[Note that, for the sake of notational simplicity, we omitted the time argument and the superscript R in the notation for these last correlation functions.]

B. Multiqubit Ramsey interference protocol

The many-body (multiqubit) Ramsey interference protocol is applicable to systems in which addressability at the single-qubit (spin) level is feasible. This protocol yields the real-space and time-resolved commutator Green's functions of spin (or, in the case of qubits, pseudospin-1/2) operators [38].

The protocol entails a special type of Rabi pulses, which can quite generally be parametrized as

$$R_n(\theta,\phi) \equiv \mathbb{1}_2\cos\frac{\theta}{2} + i\left(\sigma_n^x\cos\phi - \sigma_n^y\sin\phi\right)\sin\frac{\theta}{2}, \tag{15}$$

with $\theta = \Omega\tau$ (where Ω is the corresponding Rabi frequency and τ is the duration of the pulse), and ϕ being the phase of the laser field. The special type of such pulses of relevance for the Ramsey protocol is the one with $\theta = \pi/2$ and an arbitrary ϕ, which is hereafter denoted as $R_n(\phi)$.

Generally speaking, the Ramsey-interference protocol entails, as its first step, a local $\pi/2$-rotation at site n (with the value ϕ_1 of the parameter ϕ); this step is followed by an evolution of the system over the time interval of duration t and a local $\pi/2$-rotation at site n' or global $\pi/2$-rotation (with the value ϕ_2 of the parameter ϕ). As its final step, this protocol requires a measurement of $\sigma_{n'}^z$, i.e., the z-component of the pseudospin at site n'. Consequently, the final measurement result is given by [38]

$$M_{nn'}(\phi_1,\phi_2,t) = \langle{\rm S}(t)|\sigma_{n'}^z|{\rm S}(t)\rangle, \tag{16}$$

where $|\mathrm{S}(t)\rangle$ is the state obtained from $|\mathrm{G}_0\rangle$ after carrying out the first three steps of the Ramsey protocol:

$$|\mathrm{S}(t)\rangle \equiv R_{n'}(\phi_2)U_H(t)R_n(\phi_1)|\mathrm{G}_0\rangle. \tag{17}$$

It is straightforward to demonstrate that for a system that has the $U(1)$ symmetry under pseudospin rotations around the z axis and the one under reflections with respect to the z axis, the expression for the final measurement result in the Ramsey protocol [cf. Eq. (16)] reduces to [23]

$$M_{nn'}(\phi_1,\phi_2,t) = -\tfrac{1}{4}\big[\sin(\phi_1-\phi_2)\big(\mathcal{G}^{xx}_{nn'}+\mathcal{G}^{yy}_{nn'}\big) - \cos(\phi_1-\phi_2)\big(\mathcal{G}^{xy}_{nn'}-\mathcal{G}^{yx}_{nn'}\big)\big]. \tag{18}$$

From this last result, it can be inferred that the terms $\mathcal{G}^{xx}_{nn'}+\mathcal{G}^{yy}_{nn'}$ and $\mathcal{G}^{xy}_{nn'}-\mathcal{G}^{yx}_{nn'}$ required to determine $G^{\mathrm{R}}_{nn'}(t)$ [cf. Eq. (13)] are given by $M_{nn'}(\phi_1,\phi_2,t)$ for two different choices of the angles ϕ_1 and ϕ_2 (namely, for $\phi_1-\phi_2=\pm\pi/2$ and $\phi_1=\phi_2$, respectively).

Once the Green's functions $G^{\mathrm{R}}_{nn'}(t)$ [cf. Eq. (13)] are obtained using the above scheme, the commutator Green's function $G^{\mathrm{R}}_{-}(k,t)$ [cf. Eq. (8)] for an arbitrary quasimomentum k can be determined using a spatial Fourier transformation, whereby its anticommutator counterpart $G^{\mathrm{R}}_{+}(k,t)$ [cf. Eq. (1)] is straightforward to recover. Finally, having obtained $G^{\mathrm{R}}_{+}(k,t)$, using Eq. (4) one can compute the spectral function $A(k,\omega)$ for a broad range of frequencies through a numerical Fourier transform to the frequency domain.

IV. SIMULATOR AND ITS GOVERNING HAMILTONIAN

In what follows, we first briefly describe the layout of the SC analog simulator to be considered in the remainder of this work (Sec. IV A). We follow this up with a detailed derivation of its underlying effective Hamiltonian and its mapping to a coupled e-ph model with Peierls- and breathing-mode type e-ph interactions (Sec. IV B).

A. Layout of the analog simulator

The main building blocks of the envisioned simulator, depicted in Fig. 1, are SC qubits (Q_n), resonators (R_n), and coupler circuits (B_n) with three JJs ($n=1,\ldots,N$). The pseudospin-1/2 degree of freedom of the qubit is represented by the operators $\boldsymbol{\sigma}_n$, while microwave photons in the resonators, created (annihilated) by the operators $a^\dagger_n$ (a_n), mimic Einstein (zero-dimensional) phonons. The Hamiltonian of the nth repeating unit of the simulator, which consists of the qubit Q_n with the energy splitting ε_z and the resonator R_n with the photon frequency ω_c, is given by

$$H^0_n = \frac{\varepsilon_z}{2}\sigma^z_n + \hbar\omega_c a^\dagger_n a_n. \tag{19}$$

Qubit Q_n interacts with its nearest neighbors Q_{n-1} and Q_{n+1} through coupler circuits B_{n-1} and B_n, which represent a generalization of a SQUID loop. The total energy of B_n is given by

$$H^J_n = -\sum_{i=1}^{3} E^i_J\cos\varphi^i_n, \tag{20}$$

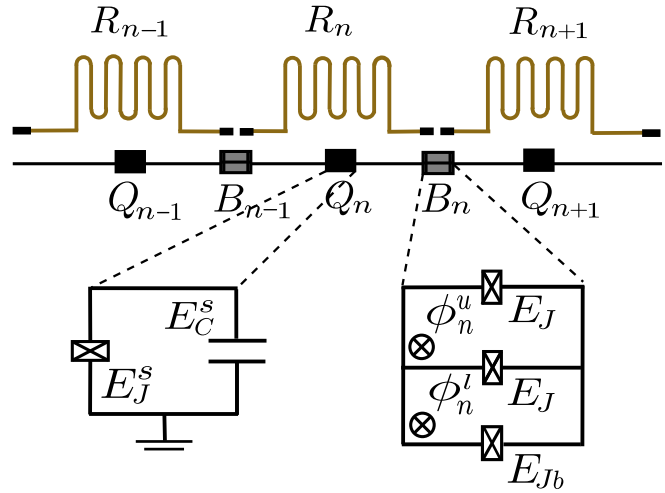

FIG. 1. Layout of the envisioned analog simulator [23], which consists of SC qubits Q_n (with single-qubit charging and Josephson energies E^s_C and E^s_J, respectively), resonators R_n, and coupler circuits B_n. Here ϕ^l_n and ϕ^u_n are the respective total magnetic fluxes threading the lower and upper loops of B_n.

where φ^i_n ($i=1,2,3$) are the phase drops on the three JJs and E^i_J their respective Josephson energies; it will hereafter be assumed that junctions 1 and 2 have the same energy (i.e., $E^1_J=E^2_J\equiv E_J$), while the third one is different from the first two (i.e., $E^3_J=E_{Jb}\neq E_J$). The qubit and resonator degrees of freedom are mutually coupled in this system through the flux of the resonator modes piercing the upper loops of coupler circuits [67]. Apart from this inductive-coupling mechanism, those circuits are also driven by a microwave radiation (ac flux) and with an external dc flux through their lower loops.

In the following, ϕ^u_n and ϕ^l_n will be used to denote the total magnetic fluxes in the upper- and lower loops of B_n, respectively. [Note that hereafter all the fluxes in the problem will be expressed in units of $\Phi_0/2\pi$, with $\Phi_0\equiv hc/(2e)$ being the flux quantum.] The flux ϕ^u_n in the upper loop includes ac-driving contribution $\pi\cos(\omega_0 t)$ and a dynamically fluctuating one from the resonator modes a_n and a_{n+1}; the latter is proportional to the difference of the photon displacement fields of resonators $n+1$ and n, i.e., $\phi_{n,\mathrm{res}}=\delta\theta_r[(a_{n+1}+a^\dagger_{n+1})-(a_n+a^\dagger_n)]$, with the constant of proportionality $\delta\theta_r$ whose value depends on the geometric properties of the specific resonator [23]. The lower-loop counterpart ϕ^l_n of ϕ^u_n also includes an ac contribution, which is given by $-(\pi/2)\cos(\omega_0 t)$. Finally, the lower-loop flux is also assumed to have a dc part ϕ_{dc}. This dc flux constitutes—aside from ω_0—the only tunable parameter in this system, hence being the principal experimental knob.

B. Effective system Hamiltonian

Due to the explicit time dependence of the ac-driving, it is favorable to switch to the rotating frame of the drive. This change of frames not only leads to a shift in the resonator (photon) frequency ($\omega_c\to\delta\omega\equiv\omega_c-\omega_0$) but also causes the Josephson-coupling term to acquire a time dependence. However, it can straightforwardly be demonstrated that this time dependence can safely be disregarded due to its rapidly

oscillating character, i.e., based on the rotating-wave approximation (RWA). After dropping those terms, the remaining part of the Josephson-coupling term is given by

$$\bar{H}_n^J = -E_n^J \cos(\varphi_n - \varphi_{n+1}), \tag{21}$$

where φ_n is the gauge-invariant phase variable corresponding to the SC island of the nth qubit [25] and

$$E_n^J = E_{Jb}(1 + \cos\phi_{\rm dc}) - E_J J_1(\pi/2)\phi_{n,\rm res}, \tag{22}$$

where $J_n(x)$ are Bessel functions of the first kind. The specific form of the last equation results from the assumption that E_{Jb} is chosen, without significant loss of generality, to be given by $2E_J J_0(\pi/2)$.

In the relevant regime for transmon qubits ($E_J^s \gg E_C^s$, where E_C^s and E_J^s are the charging and Josephson energies of a single qubit, respectively), it is permissible to expand $\cos(\varphi_n - \varphi_{n+1})$ up to the second order in $\varphi_n - \varphi_{n+1}$, where this expansion is controlled by the small parameter $\delta\varphi_0^2 \equiv (2E_C^s/E_J^s)^{1/2}$ (the quantum displacement of the gauge-invariant phase); for a typical transmon qubit ($E_J^s/E_C^s \sim 100$) one finds $\delta\varphi_0^2 \sim 0.15$. Importantly, higher powers of $\varphi_n - \varphi_{n+1}$ in that expansion can be neglected not only because of the smallness of this phase difference, but also due to the rapidly decreasing coefficients in the expansion, which are proportional to higher powers of $\delta\varphi_0^2$. By switching to the pseudospin-1/2 operators $\boldsymbol{\sigma}_n$, $\cos(\varphi_n - \varphi_{n+1})$ can be rewritten (up to an additive constant, which is irrelevant for our present purposes) in the form (for a detailed derivation, see Appendix A)

$$\cos(\varphi_n - \varphi_{n+1}) \approx \delta\varphi_0^2\left[\sigma_n^+\sigma_{n+1}^- + \sigma_n^-\sigma_{n+1}^+ - \frac{\sigma_n^z + \sigma_{n+1}^z}{2}\right]. \tag{23}$$

The first term on the right-hand side of the last equation corresponds to an XY-type coupling between two adjacent transmons, while the second one—being of the same form as the σ_n^z term in Eq. (19)—describes a shift in their (single-qubit) frequency.

It is worthwhile mentioning that in the derivation of Eq. (23), the terms of the type $\sigma_n^+\sigma_{n+1}^+$ and $\sigma_n^-\sigma_{n+1}^-$ have been neglected. While this is conventionally done—by virtue of the RWA—even in the most general (multilevel) treatment of transmons, in the problem at hand there is an even more rigorous argument for doing so. Namely, here we are concerned with a single-excitation polaron problem. Therefore, the part of the total Hilbert space of relevance for this problem consists of states with a single spinless fermion, which in the pseudospin-1/2 (qubit) language translates into states with precisely one qubit in the logical state $|1\rangle$. Accordingly, the terms $\sigma_n^-\sigma_{n+1}^-$ and $\sigma_n^+\sigma_{n+1}^+$ both yield zero when acting on an arbitrary state in the relevant part of the Hilbert space of the system.

At this point, it is pertinent to recast the problem at hand in terms of the spinless-fermion operators $\{c_n, c_n^\dagger\}$ (instead of the pseudospin-1/2 operators $\boldsymbol{\sigma}_n$) via the JW transformation [cf. Eq. (12)], whereby $\sigma_n^+\sigma_{n+1}^- + \sigma_n^-\sigma_{n+1}^+ \to c_n^\dagger c_{n+1} + \text{H.c.}$ This allows us to write the effective system Hamiltonian in the form of a lattice model that describes an itinerant spinless-fermion excitation interacting with zero-dimensional bosons (phonons) through two different e-ph coupling mechanisms.

The noninteracting (free) part H_0 of the effective system Hamiltonian consists of the free-excitation (hopping) and free-phonon terms

$$H_0 = -t_0(\phi_{\rm dc})\sum_n (c_n^\dagger c_{n+1} + \text{H.c.}) + \hbar\delta\omega\sum_n a_n^\dagger a_n, \tag{24}$$

where $t_0(\phi_{\rm dc}) \equiv E_{Jb}\delta\varphi_0^2(1 + \cos\phi_{\rm dc})$ plays the role of the effective bare-excitation hopping amplitude. This hopping amplitude can be tuned by varying the dc flux $\phi_{\rm dc}$. [Strictly speaking, H_0 also contains diagonal terms $c_n^\dagger c_n$, which originate from the terms with σ_n^z in Eq. (19), as well as from the expansion of $\cos(\varphi_n - \varphi_{n+1})$. Yet, these terms can be disregarded as they only lead to a band offset for spinless fermions.] On the other hand, the interacting part includes two e-ph coupling terms and is given by [68]

$$H_{\text{e-ph}} = g\hbar\delta\omega l_0^{-1}\sum_n [(c_n^\dagger c_{n+1} + \text{H.c.})(u_{n+1} - u_n) - c_n^\dagger c_n(u_{n+1} - u_{n-1})], \tag{25}$$

where g is the dimensionless e-ph coupling strength and $u_n \equiv l_0(a_n + a_n^\dagger)$, with l_0 being the zero-point length of the Einstein oscillator with frequency $\delta\omega$. The first term corresponds to the Peierls-coupling mechanism, which accounts for the lowest-order (linear) dependence of the effective (phonon-modulated) hopping amplitude between sites n and $n+1$ on the difference $u_{n+1} - u_n$ of the corresponding phonon displacements [45]. The second term corresponds to the breathing-mode type coupling [46], i.e., the antisymmetric coupling of the excitation density $c_n^\dagger c_n$ at site n with the phonon displacements on sites $n \pm 1$.

When recast in momentum space, $H_{\text{e-ph}}$ assumes the form $N^{-1/2}\sum_{k,q}\gamma_{\text{e-ph}}(k,q)c_{k+q}^\dagger c_k(a_{-q}^\dagger + a_q)$, where

$$\gamma_{\text{e-ph}}(k,q) = 2ig\hbar\delta\omega[\sin k + \sin q - \sin(k+q)] \tag{26}$$

is the corresponding e-ph vertex function [note that here quasimomenta are expressed in units of the inverse lattice constant, thus the quasimomenta from the Brillouin zone belong to $(-\pi, \pi]$]. For the most general (momentum-dependent) vertex function $\gamma_{\text{e-ph}}(k,q)$, the effective e-ph coupling strength is given by

$$\lambda_{\rm eff} = \frac{\langle|\gamma_{\text{e-ph}}(k,q)|^2\rangle}{2t_{\rm e}\hbar\omega_{\rm ph}}, \tag{27}$$

where $t_{\rm e}$ is the excitation hopping amplitude, $\omega_{\rm ph}$ is the phonon frequency, and $\langle\cdots\rangle$ stands for the Brillouin-zone average over quasimomenta k and q:

$$\langle|\gamma_{\text{e-ph}}(k,q)|^2\rangle \equiv \frac{1}{(2\pi)^2}\int_{-\pi}^{\pi}\int_{-\pi}^{\pi}|\gamma_{\text{e-ph}}(k,q)|^2 dk dq. \tag{28}$$

In the problem at hand—where $t_{\rm e} \to t_0$, $\omega_{\rm ph} \to \delta\omega$, and the vertex function is given by Eq. (26)—the effective coupling strength evaluates to $\lambda_{\rm eff} \equiv 3g^2\hbar\delta\omega/t_0$ and depends on $\phi_{\rm dc}$.

The fact that the vertex function in Eq. (26) depends both on q and k implies that the Hamiltonian $H_{\rm eff} = H_0 + H_{\text{e-ph}}$ does not belong to the realm of applicability of the

Gerlach-Löwen theorem [58], which rules out a nonanalytic behavior of ground-state-related quantities. It was already demonstrated that the ground state of this Hamiltonian displays a sharp (level-crossing) transition at a critical value of the effective coupling strength (tuned here by varying $\phi_{\rm dc}$) [23]. Whereas below the critical value the system has a zero-quasimomentum ground state—that is, the energy minimum corresponds to the eigenvalue $K = 0$ of the total quasimomentum operator

$$K_{\rm tot} = \sum_k k c_k^\dagger c_k + \sum_q q a_q^\dagger a_q, \tag{29}$$

above this critical value $H_{\rm eff}$ has a twofold-degenerate ground state. This unconventional, degenerate ground state corresponds to the pair of equal and opposite (nonzero) quasimomenta $\pm K_{\rm gs}$, where $K_{\rm gs}$ reaches the value of $\pi/2$ for a sufficiently strong coupling (i.e., sufficiently large $\lambda_{\rm eff}$).

It is worthwhile pointing out that the system at hand has the peculiar property that the $k = 0$ Bloch state $|\Psi_{k=0}\rangle \equiv c_{k=0}^\dagger |0\rangle_{\rm e} \otimes |0\rangle_{\rm ph}$ of a bare excitation is an exact eigenstate of $H_{\rm eff}$ for an arbitrary coupling strength, regardless of the value of $\lambda_{\rm eff}$. This fact has profound consequences for the resulting spectral function (cf. Sec. V below). Moreover, for effective coupling strengths $\lambda_{\rm eff}$ below the critical one, $|\Psi_{k=0}\rangle$ is the lowest-energy eigenstate of $H_{\rm eff}$, i.e., its ground state. The state $|\Psi_{k=0}\rangle$, when recast in terms of pseudospin-1/2 (qubit) degrees of freedom via the JW transformation [cf. Eq. (12)], corresponds to an N-qubit W state [68]; more generally, the bare-excitation Bloch state $|\Psi_k\rangle$ with quasimomentum k corresponds to a twisted N-qubit W state [69].

The dimensionless e-ph coupling strength g [cf. Eq. (25)] is given by $g\hbar\delta\omega = \delta\varphi_0^2 E_J J_1(\pi/2)\delta\theta_r$. While g itself does not depend on ω_0 and $\phi_{\rm dc}$, $\lambda_{\rm eff}$ inherits the dependence on the latter parameter from t_0 and can thus be tuned by varying $\phi_{\rm dc}$. More precisely, the effective e-ph coupling strength has the following dependence on the dc flux:

$$\lambda_{\rm eff}(\phi_{\rm dc}) = \frac{3}{2} g \frac{J_1(\pi/2)\delta\theta_r}{J_0(\pi/2)(1+\cos\phi_{\rm dc})}. \tag{30}$$

For a typical SC microwave resonator, the value of $\delta\theta_r$ is around 3.5×10^{-3}, while the effective phonon frequency $\delta\omega$ can be taken to be in the range $\delta\omega/2\pi = 200$–300 MHz. By choosing the Josephson energy E_J such that the condition $\delta\varphi_0^2 E_J/2\pi\hbar = 100\,{\rm GHz}$ is satisfied, one obtains $g\delta\omega/2\pi = 198$ MHz.

The system under consideration allows one to access both the adiabatic ($t_0 > \hbar\delta\omega$) and antiadiabatic regime ($t_0 < \hbar\delta\omega$) of small-polaron physics by varying $\phi_{\rm dc}/\pi$ in the fairly narrow range 0.95–0.99. For the choice $\delta\omega/2\pi = 200\,{\rm MHz}$ of the effective phonon frequency, for instance, the onset of the antiadiabatic regime is for $\phi_{\rm dc}/\pi \approx 0.980$. For the same choice of parameters, the sharp ground-state transition takes place for $\phi_{\rm dc}/\pi \approx 0.968$, the corresponding value of the effective coupling strength $\lambda_{\rm eff}$ being approximately equal to 1.24. Importantly, in the same narrow range of values for $\phi_{\rm dc}$, $\lambda_{\rm eff}$ can assume both values within the weak-coupling regime (e.g., for $\delta\omega/2\pi = 200\,{\rm MHz}$ and $\phi_{\rm dc}/\pi = 0.95$, one finds the effective coupling strength $\lambda_{\rm eff} = 0.51$) and in the strong-coupling one (e.g., for $\delta\omega/2\pi = 200\,{\rm MHz}$ and $\phi_{\rm dc}/\pi = 0.98$ one obtains $\lambda_{\rm eff} = 3.17$).

Both bare-excitation and dressed-excitation Bloch states can be prepared in the system at hand, starting from the initial state $|{\rm G}_0\rangle$, using a microwave-driving protocol proposed in Ref. [23]. This protocol, which is based on the discrete translational symmetry of the system and energy conservation, allows the preparation of the desired Bloch states within times 3–4 orders of magnitude shorter than the currently achievable decoherence times T_2 of SC qubits.

V. RESULTS AND DISCUSSION

Using the KPM (for the essential aspects of this computational scheme, see Appendix C), the single-particle spectral function [cf. Eq. (5)] was evaluated for a system with $N = 10$ sites and the total of $N_{\rm ph}^{\rm max} = 18$ phonons in the truncated phonon Hilbert space; the dimension of the latter Hilbert space is $D_{\rm ph} = 43,758$ (for general aspects of the Hilbert-space truncation, see Appendix B). To achieve a good resolution, we evaluated as many as 10^5 Chebyshev moments (cf. Appendix C) in the expansion of the desired spectral function $A(k,\omega)$.

Our KPM-based evaluation of the momentum-frequency resolved spectral function was carried out on a 64-core, 7 GHz AMD Ryzen Threadripper PRO 5995WX workstation, with a total of 527GB of main memory. The runs that were needed to obtain the results presented in this section consumed around 50 h.

The evaluation was carried out for three different values of the dc flux $\phi_{\rm dc}$, the main experimental knob in the system, two of which belong to the antiadiabatic regime ($\phi_{\rm dc}/\pi = 0.95$ and 0.97) and one to the adiabatic one ($\phi_{\rm dc}/\pi = 0.98$). The resulting frequency dependence of the spectral function for six different quasimomenta ($k = 0, \pi/5, 2\pi/5, 3\pi/5, 4\pi/5, \pi$) in the positive half of the Brillouin zone, consistent with periodic boundary conditions, is depicted in Figs. 2–4. In each particular case, it was numerically verified that the obtained spectral function satisfies the sum rule in Eq. (6).

To understand the obtained results, it is useful to recall some general properties of the energy spectra of models describing a short-range coupling of an itinerant excitation with dispersionless phonons; the strong-coupling regime of such models is characterized by the presence of heavily dressed excitations (small polarons). Regardless of the specific form of the e-ph interaction, the center of the small-polaron Bloch band is situated at an energy E_b below that of a bare excitation, this last energy being referred to as the small-polaron binding energy.

At a fixed quasimomentum k, the sum over eigenstates that contributes to the spectral function includes the discrete states (i.e., those that belong to coherent polaron Bloch bands) and their respective continua; importantly, the energetic width of each of those continua is equal that of the respective polaron Bloch band. In particular, the one-phonon continuum represents the inelastic-scattering threshold—i.e., the minimal energy that a phonon-dressed excitation ought to have to be capable of emitting a single phonon. This one-phonon continuum sets in at the energy $\hbar\omega_{\rm ph}$ above the ground-state

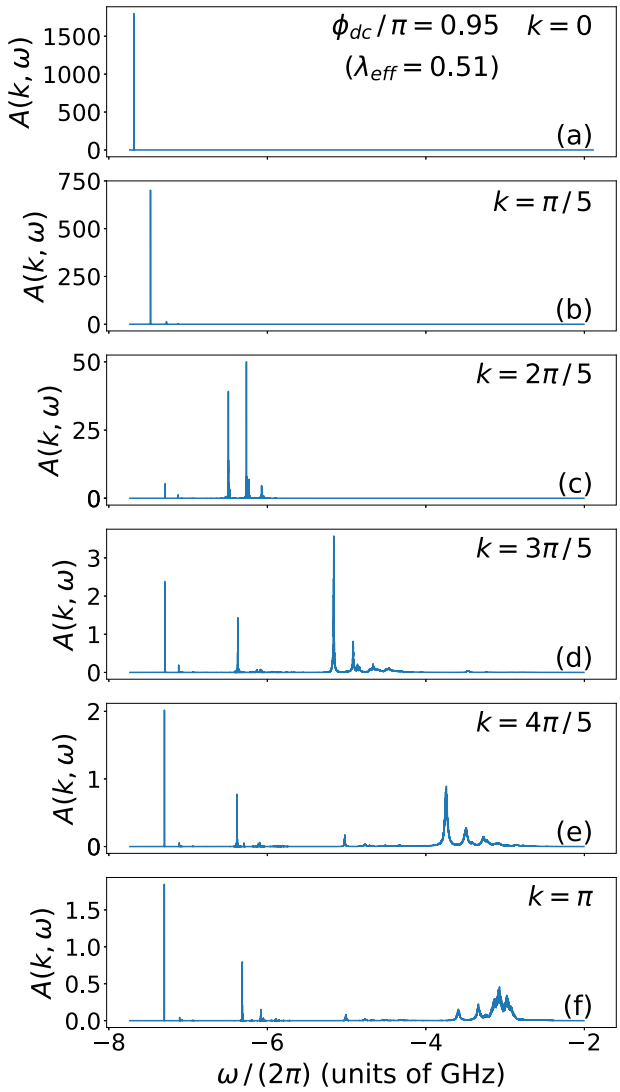

FIG. 2. Momentum-frequency resolved spectral function $A(k, \omega)$ for six different quasimomenta k in the Brillouin zone, evaluated for a range of frequencies. The parameter values used are $\delta\omega/(2\pi) = 200\,\text{MHz}$ and $\phi_{\text{dc}}/\pi = 0.95$; the corresponding effective coupling strength is $\lambda_{\text{eff}} = 0.51$. The obtained spectral function satisfies the sum rule in Eq. (6).

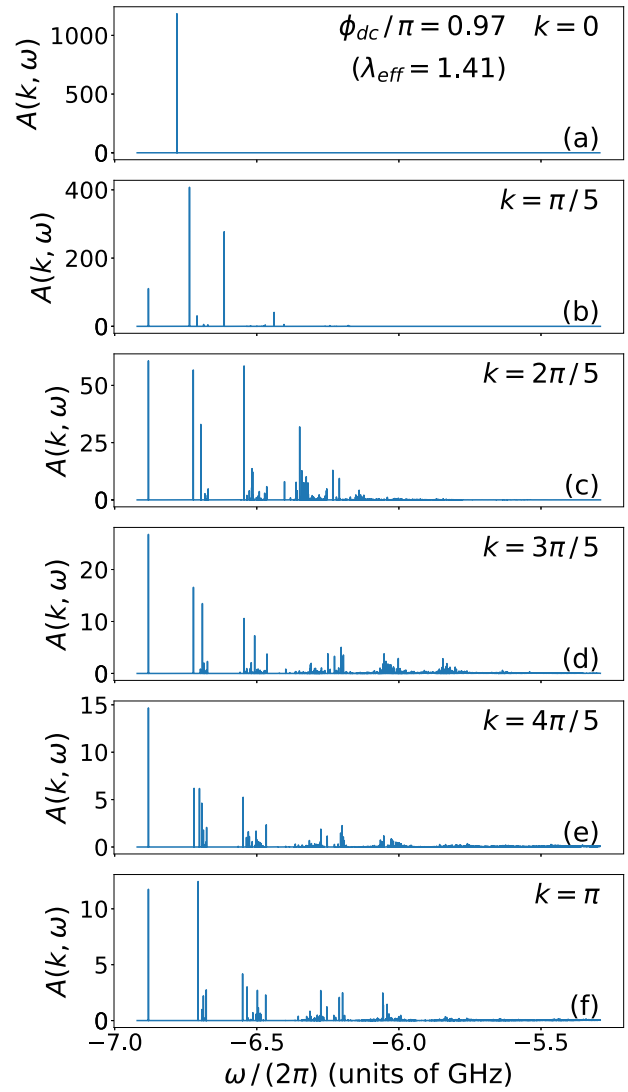

FIG. 3. Momentum-frequency resolved spectral function $A(k, \omega)$ for six different quasimomenta k in the Brillouin zone, evaluated for a range of frequencies. The parameter values used are $\delta\omega/(2\pi) = 200\,\text{MHz}$ and $\phi_{\text{dc}}/\pi = 0.97$; the corresponding effective coupling strength is $\lambda_{\text{eff}} = 1.41$. The obtained spectral function satisfies the sum rule in Eq. (6).

energy, where ω_{ph} is the phonon frequency [70] (recall that in the system at hand, the role of the effective phonon frequency is played by $\delta\omega$). For a sufficiently weak e-ph coupling, a coupled e-ph system only has one discrete Bloch state $|\psi_k^{(j=0)}\rangle$ at quasimomentum k, and its corresponding continuum of states pertains to a dressed excitation with quasimomentum $k - q$ and an unbound phonon with quasimomentum q.

As the e-ph coupling strength is increasing, additional coherent polaron bands—i.e., additional discrete states at each quasimomentum k in the Brillouin zone—start to emerge below the aforementioned one-phonon continuum. The first such excited polaron state at quasimomentum k—split off from the continuum—corresponds to a polaron bound with an additional phonon, their total quasimomentum being equal to k. For even stronger e-ph coupling there is another, second excited state, which represents a bound state of a polaron and two additional phonons (again, with the same total quasimomentum k). Those states, along with their respective continua, provide additional contributions to the spectral function $A(k, \omega)$ [71].

For the lowest value used (0.95) of the parameter ϕ_{dc}/π, the system is in the weak-coupling regime—below the sharp ground-state transition. As pointed out in Sec. IV B, its ground state corresponds to a bare-excitation Bloch state at quasimomentum $k = 0$, which explains the presence of a single discrete peak of the spectral function $A(k = 0, \omega)$ in Fig. 2. For larger quasimomenta k, new peaks, which correspond to excited dressed-excitation (polaron) Bloch states, gradually appear.

In keeping with general characteristics of energy spectra of coupled e-ph systems, for increasing values of ϕ_{dc}/π, which in the system under consideration translate into a larger value of the effective e-ph coupling strength [cf. Eq. (30)], one can

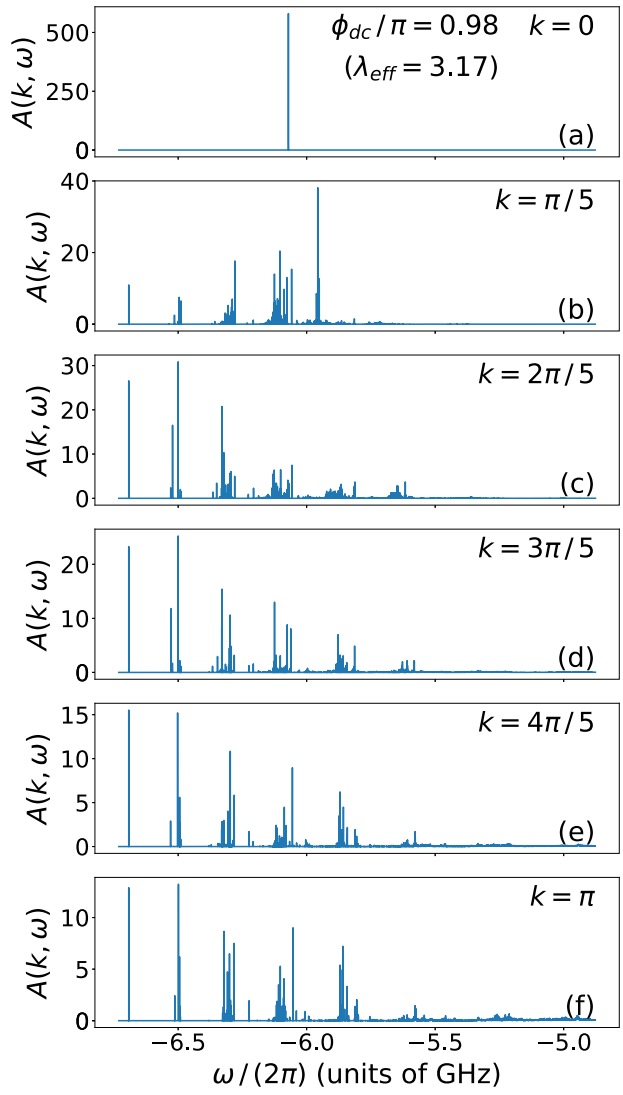

FIG. 4. Momentum-frequency resolved spectral function $A(k, \omega)$ for six different quasimomenta k in the Brillouin zone, evaluated for a range of frequencies. The parameter values used are $\delta\omega/(2\pi) = 200\,\mathrm{MHz}$ and $\phi_{\mathrm{dc}}/\pi = 0.98$; the corresponding effective coupling strength is $\lambda_{\mathrm{eff}} = 3.17$. The obtained spectral function satisfies the sum rule in Eq. (6).

notice an increasing number of discrete peaks. In particular, it can be inferred from Figs. 3 and 4 that up to the largest effective coupling strength considered ($\lambda_{\mathrm{eff}} = 3.17$), there are up to five such peaks, accompanied by their corresponding continua.

The salient feature of the obtained results for the spectral function at $k = 0$ for all four values of ϕ_{dc}/π is the absence of the one-phonon continuum. This, seemingly peculiar, result is a direct consequence of the fact that—due to equal Peierls- and breathing-mode coupling strengths in the system at hand—the free-excitation Bloch state with quasimomentum $k = 0$ represents an exact eigenstate of the total system Hamiltonian at an arbitrary coupling strength (cf. Sec. IV B). In other words, while only for ϕ_{dc}/π below the critical value of around 0.968 is this state the ground state of the system, it represents an eigenstate even above the transition point where the ground state itself no longer corresponds to the

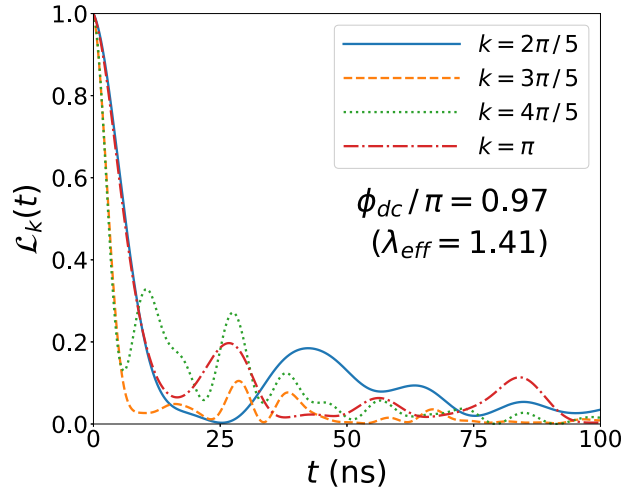

FIG. 5. Time dependence of the Loschmidt echo for four different initial free-excitation quasimomenta ($k = 2\pi/5, 3\pi/5, 4\pi/5$, and π). The parameter values used are the same as in Fig. 3.

total quasimomentum $K = 0$ but instead to a pair of nonzero quasimomenta $\pm\pi/2$. This last circumstance also explains why in Figs. 3 and 4 the only discrete peak for $k = 0$ [part (a) of the respective figure] appears at a higher energy than the lowest-lying peaks at other quasimomenta [parts (b)–(f) of the respective figure].

Having described the obtained results for the spectral function, it is useful to point out the connection between the computed spectral properties and nonequilibrium dynamics of the coupled e-ph system [72]. As mentioned above (cf. Sec. II), the spectral function $A(k, \omega)$ is simply related—by a Fourier transform in time—to the Loschmidt amplitude $\langle\psi(t)|c_k^\dagger|0\rangle$ for the system to remain at time t in the initial, bare-excitation state with quasimomentum k. In a typical situation—with a few discrete δ-like peaks (i.e., Bloch bands of a dressed excitation) accompanied by their respective continua, approximately represented as Lorentzians—this can allow one to get a qualitative picture of the system dynamics.

Namely, knowing that the Fourier transform to the time domain of a frequency-space Lorentzian is the bilateral exponential function $e^{-|t|/\tau}$ [where τ is the inverse half-width at half-maximum (HWHM) of the Lorentzian], one can straightforwardly find the survival probability of the original bare-excitation state with quasimomentum k (the Loschmidt echo) $\mathcal{L}_k(t)$ at time t [cf. Eq. (7)]. For instance, in the simplest case of a single sharp peak and its corresponding continuum, the latter is given by a sum of a constant (time-independent) term, an exponentially decaying one, and an exponentially damped oscillatory term. In cases with multiple peaks and their respective continua, the resulting expression for the Loschmidt echo is more complicated, as it involves multiple oscillatory terms, but it is still straightforward to derive.

The typical decaying oscillatory behavior of the Loschmidt echo is illustrated in Fig. 5. The rapid decay of this quantity as a function of time t after an e-ph interaction quench reflects the fact that the initially bare itinerant excitation becomes increasingly phonon-dressed over time. On the other hand, the oscillatory features of this quantity originate from the fact

that the initial bare-excitation Bloch state $c_k^\dagger|0\rangle$ at a generic quasimomentum k is not an eigenstate of the coupled e-ph Hamiltonian of the system (i.e., the Hamiltonian describing the postquench dynamics), but is rather given by a linear combination of multiple eigenstates of this Hamiltonian (recall, however, that the system at hand has a rather unconventional property that the $k = 0$ bare-excitation Bloch state is its exact eigenstate for an arbitrary e-ph coupling strength; consequently, the dynamics for $k = 0$ are completely trivial). This oscillatory behavior of the Loschmidt echo can be recovered more accurately by directly solving the Schrödinger equation for a phonon-dressed excitation using a Chebyshev expansion of its time-evolution operator [24].

For completeness, it is of interest to comment on the capability of the proposed SC system for accurate measurements of the momentum-frequency resolved spectral function of dressed excitations in the underlying coupled e-ph model (cf. Sec. II) and, by extension, elucidating quantum dynamics of the small-polaron formation. The actual resolution with which the retarded single-particle Green's function can be determined using the many-body version of the Ramsey interference protocol (cf. Sec. III B) is certainly setup-specific, i.e., dependent on the specific data-acquisition capabilities available. Accordingly, the frequency resolution that can be achieved in an experimental realization of our proposal for measuring the spectral function will also be dependent on the specific setup. However, a general argument can be provided as to why accurate measurements of the spectral function—as well as drawing quantitative conclusions about the small-polaron formation dynamics—in the proposed system is conceivable with existing technology.

Namely, the characteristic energy scales in the proposed SC analog simulators are three to four orders of magnitude smaller than their counterparts in solid-state systems. For instance, the frequencies of microwave photons that emulate phonons in this system are of the order of 0.1GHz, while a typical optical-phonon frequency in the solid state is of the order of a few THz. As a result, the dynamics of our proposed system are three to four orders of magnitude slower than that of its solid-state counterparts, which—in fact—is the principal reason why such analog simulators can be put to good use in elucidating complex dynamical processes. For this reason, assuming similar technological capabilities in both cases, we can conclude that it should actually be more straightforward to measure the relevant dynamical response functions accurately in the proposed synthetic SC system than in naturally occurring electronic materials.

VI. SUMMARY AND CONCLUSIONS

In this paper, we proposed a scheme for investigating the spectral properties of polaronic excitations using a superconducting analog simulator based on an array of inductively coupled superconducting qubits and microwave resonators. This system emulates a model describing an itinerant spinless-fermion excitation coupled to dispersionless phonons via Peierls- and breathing-mode type excitation-phonon interactions. Using the kernel polynomial method, we computed the momentum-frequency resolved spectral function of this system for several different choices of its parameters, covering both the adiabatic and antiadiabatic regimes of this model. In addition, we indicated how this spectral function can be recovered experimentally using the many-body version of the Ramsey interference protocol.

We found implications of strong, nonlocal excitation-phonon coupling in the investigated system for its spectral properties. A salient feature of this system—resulting from the fact that Peierls' and breathing-mode coupling strengths in this system are equal—is that its single-particle spectral function does not show a one-phonon continuum at zero quasimomentum. This is a direct implication of the fact that the bare-excitation Bloch state with zero-quasimomentum is an exact eigenstate of the coupled excitation-phonon Hamiltonian of the system for an arbitrary excitation-phonon coupling strength.

The present study of spectral properties can be extended to other types of analog simulators [73]. Namely, essentially the same coupled e-ph model can be experimentally realized as an analog simulator based on an array of neutral atoms in optical tweezers that interact through Rydberg-dressed resonant dipole-dipole interaction [74]. Therefore, the same experimental investigation of the spectral properties of polarons born out of the interplay of Peierls' and breathing-mode type e-ph interactions can also be carried out using that atomic system, with the added benefit that this last system allows one to independently vary both coupling strengths.

ACKNOWLEDGMENTS

This research was supported by the Deutsche Forschungsgemeinschaft (DFG) – SFB 1119 – 236615297.

APPENDIX A: DERIVATION OF EQ. (23)

In what follows, we provide the derivation of the approximate expression for $\cos(\varphi_n - \varphi_{n+1})$ [Eq. (23) in Sec. IV B] in the regime of interest for transmon qubits.

We start from the quantization of the gauge-invariant phase variables φ_n in terms of bosonic operators [17]

$$\varphi_n = \delta\varphi_0(b_n + b_n^\dagger), \tag{A1}$$

where $\delta\varphi_0 \equiv (2E_C^s/E_J^s)^{1/4}$. In the regime of relevance for transmons ($E_J^s/E_C^s \sim 100$), it is pertinent to expand $\cos(\varphi_n - \varphi_{n+1})$ to the second order in the phase difference $\varphi_n - \varphi_{n+1}$, where $\delta\varphi_0$ plays the role of the small parameter controlling the expansion. In this manner, by also making use of Eq. (A1), we readily obtain

$$\cos(\varphi_n - \varphi_{n+1}) \approx 1 - \tfrac{1}{2}\delta\varphi_0^2[(b_n + b_n^\dagger)^2 - (b_{n+1} + b_{n+1}^\dagger)^2]. \tag{A2}$$

By exploiting bosonic commutation relations for the operators b_n, $b_n^\dagger$, b_{n+1}, and $b_{n+1}^\dagger$, we further find

$$\begin{aligned}\cos(\varphi_n - \varphi_{n+1}) \approx 1 &- \frac{\delta\varphi_0^2}{2}(b_n^\dagger b_n + b_{n+1}^\dagger b_{n+1} + 1) \\ &+ \frac{\delta\varphi_0^2}{2}(b_n b_{n+1} + b_n b_{n+1}^\dagger + b_n^\dagger b_{n+1} \\ &+ b_n^\dagger b_{n+1}^\dagger).\end{aligned} \tag{A3}$$

While up to this point the transformations were completely general, i.e., consistent with the multilevel treatment of transmon qubits, we now resort to the two-level approximation and switch from the bosonic operators b_n, $b_n^\dagger$ to the pseudospin-1/2 operators $\boldsymbol{\sigma}_n$ representing transmons; in the two-level approximation, the bosonic occupation numbers are constrained to 0 and 1. This transformation from constrained bosonic to pseudospin operators can be seen as an inverted version of the Holstein-Primakoff transformation in solid-state physics [75]. In the lowest order of this transformation in the spin-1/2 case, we have

$$b_n \to \sigma_n^+, \quad b_n^\dagger \to \sigma_n^-, \quad b_n^\dagger b_n \to \tfrac{1}{2}\big(1-\sigma_n^z\big). \tag{A4}$$

Using this last transformation, Eq. (A3) can be recast as

$$\begin{aligned}\cos(\varphi_n-\varphi_{n+1}) \approx 1 &- \frac{\delta\varphi_0^2}{4}\big(4-\sigma_n^z-\sigma_{n+1}^z\big)\\ &+\frac{\delta\varphi_0^2}{2}(\sigma_n^+\sigma_{n+1}^+ + \sigma_n^+\sigma_{n+1}^-\\ &+\sigma_n^-\sigma_{n+1}^+ + \sigma_n^-\sigma_{n+1}^-).\end{aligned} \tag{A5}$$

The terms $\sigma_n^+\sigma_{n+1}^+$ and $\sigma_n^-\sigma_{n+1}^-$ in the last expression can be neglected by virtue of the RWA. While this is conventionally done even in the most general (multilevel) treatment of transmons, in the single-fermion problem at hand such terms invariably yield zero when they act on states in the relevant part of the Hilbert space of the system (i.e., multiqubit states with only one qubit in the logical $|1\rangle$ state). By also disregarding the constant term $1-\delta\varphi_0^2$ in Eq. (A5), which is immaterial in the present physical context, we obtain the final expression for $\cos(\varphi_n-\varphi_{n+1})$ [cf. Eq. (23)]:

$$\cos(\varphi_n-\varphi_{n+1}) \approx \delta\varphi_0^2\left[\sigma_n^+\sigma_{n+1}^- + \sigma_n^-\sigma_{n+1}^+ - \frac{\sigma_n^z+\sigma_{n+1}^z}{2}\right]. \tag{A6}$$

APPENDIX B: HILBERT-SPACE TRUNCATION AND SYMMETRY-ADAPTED BASIS

The basis of the Hilbert space $\mathcal{H}_{\text{e-ph}} = \mathcal{H}_\text{e} \otimes \mathcal{H}_\text{ph}$ of the coupled e-ph system under consideration is given by $|n\rangle_e \otimes |\mathbf{m}\rangle_\text{ph}$, with the states $|n\rangle_e \equiv c_n^\dagger|0\rangle_e$ that correspond to the excitation localized at the site n ($n=1,\ldots,N$) and the phonon state $|\mathbf{m}\rangle_\text{ph}$ with the occupation numbers $\mathbf{m} \equiv (m_1,\ldots,m_N)$ at different sites:

$$|\mathbf{m}\rangle_\text{ph} = \prod_{n=1}^{N\otimes} \frac{(b_n^\dagger)^{m_n}}{\sqrt{m_n!}}|0\rangle_\text{ph}. \tag{B1}$$

Given that the phonon Hilbert space is infinite-dimensional, we restrict ourselves to the truncated phonon Hilbert space. The latter includes states with the total number of phonons $m=\sum_{n=1}^N m_n$ (where $0 \leqslant m_n \leqslant m$) not larger than N_ph^max. Consequently, the dimension of the total e-ph Hilbert space is $D = D_\text{e} \times D_\text{ph}$, where $D_\text{e} = N$ and $D_\text{ph} = (N_\text{ph}^\text{max}+N)!/(N_\text{ph}^\text{max}!N!)$.

The problem of diagonalizing the Hamiltonian of the coupled e-ph system under consideration can further be simplified by exploiting the discrete translational symmetry of this system. This symmetry is mathematically expressed by the commutation $[H_\text{eff}, K_\text{tot}] = 0$ of the Hamiltonian H_eff of the system and the total quasimomentum operator K_tot. Due to this symmetry, one has to diagonalize H_eff in the sectors of $\mathcal{H}_\text{e-ph}$ that correspond to the eigensubspaces of K_tot; the dimension of each of those K-sectors of the total Hilbert space is equal that of the truncated phonon space, i.e., $D_K = D_\text{ph}$. Accordingly, one makes use of the symmetry-adapted basis,

$$|K,\mathbf{m}\rangle = N^{-1/2}\sum_{n=1}^N e^{iKn}\,\mathcal{T}_n(|1\rangle_\text{e}\otimes|\mathbf{m}\rangle_\text{ph}), \tag{B2}$$

of $\mathcal{H}_\text{e-ph}$, where $\mathcal{T}_n$ are the discrete-translation operators; the action of these operators has to comply with the periodic boundary conditions. The last equation can be rewritten in the form

$$|K,\mathbf{m}\rangle = N^{-1/2}\sum_{n=1}^N e^{iKn}\,|n\rangle_\text{e}\otimes\mathcal{T}_n^\text{ph}|\mathbf{m}\rangle_\text{ph}, \tag{B3}$$

with the operators $\mathcal{T}_n^\text{ph}$ representing discrete translations in the phonon Hilbert space. If $|\mathbf{m}\rangle_\text{ph}$ is defined by a set of occupation numbers

$$|\mathbf{m}\rangle_\text{ph} = |m_1, m_2, \ldots, m_N\rangle_\text{ph}, \tag{B4}$$

it is straightforward to show that $\mathcal{T}_n^\text{ph}|\mathbf{m}\rangle_\text{ph} \equiv |\mathcal{T}_n^\text{ph}\mathbf{m}\rangle$ is given by

$$\big|\mathcal{T}_n^\text{ph}\mathbf{m}\big\rangle = |m_{N-n+1}, m_{N-n+2}, \ldots, m_{N-n}\rangle_\text{ph}. \tag{B5}$$

APPENDIX C: SPECTRAL-FUNCTION EVALUATION USING THE KPM

1. Basic aspects of the KPM

In the following, we briefly recapitulate the basic aspects of the kernel polynomial method (KPM) [34], as well as the most relevant details of our concrete implementations thereof. A more detailed introduction into the KPM and its applications in many-body physics can be found in Ref. [33].

In the following, we summarize the basic aspects of the KPM along with the most relevant details of our own implementation of this approach for the purpose of calculating momentum-frequency resolved spectral function.

At the heart of the KPM lies the problem of approximating a real-valued function $f(x)$ [76] defined on the interval $[-1,1]$ by a finite series of Chebyshev polynomials $T_n(x)$ of the first kind ($n=0,\ldots,N_\text{C}-1$):

$$f^{(N_\text{C})}(x) = \frac{1}{\pi\sqrt{1-x^2}}\left[\mu^{(0)} + 2\sum_{n=1}^{N_\text{C}-1}\mu^{(n)}T_n(x)\right]. \tag{C1}$$

The coefficients $\mu^{(n)}$ in the above expansion, referred to as Chebyshev moments, are given by

$$\mu^{(n)} = \int_{-1}^{1} f(x)T_n(x)dx. \tag{C2}$$

For a sufficiently smooth function $f(x)$ the last series converges uniformly to f on any closed subinterval of $[-1,1]$ that excludes the end points ±1.

When the function to be approximated is not continuous or—as is very common in physics applications such as the present one—has peaks associated with quasiparticle states with infinite lifetime, the series in Eq. (C1) cannot converge uniformly. Namely, it fails to converge in the vicinity of a discontinuity, showing instead rapid oscillations whose amplitude does not decrease as the number of terms in the series goes to infinity (the Gibbs phenomenon) [77].

In particular, it was proven that the problem arising from the Gibbs phenomenon is solved for Chebyshev expansions. Namely, for any fixed number N_C of terms in the expansion it is possible to specify a set of attenuation factors $g_n^{N_C}$ ($n = 0, \ldots, N_C - 1$), such that the modified finite-series approximants

$$f^{(N_C)}(x) = \frac{1}{\pi\sqrt{1-x^2}}\left[g_0^{N_C}\mu^{(0)} + 2\sum_{n=1}^{N_C-1} g_n^{N_C}\mu^{(n)}T_n(x)\right] \tag{C3}$$

do not display the Gibbs phenomenon, providing instead accurate approximations to a broad class of functions. In other words, the introduction of the attenuation factors $g_n^{N_C}$ damps out high-frequency oscillations—that would otherwise cause spurious results—and constitutes the essential ingredient of the KPM.

In the problem at hand, we utilize factors $g_n^{N_C}$ derived from the Jackson kernel [78]. The explicit form of those factors reads [79]

$$g_n^{N_C} = \frac{1}{N_C+1}\left\{(N_C - n + 1)\cos\left(\frac{n\pi}{N_C+1}\right) + \sin\left(\frac{n\pi}{N_C+1}\right)\cot\left(\frac{\pi}{N_C+1}\right)\right\}. \tag{C4}$$

2. Evaluation of the spectral function $A(k, \omega)$

In the present work, the KPM is utilized to evaluate the momentum-frequency resolved spectral function, given by Eq. (4). To this end, the spectrum of the total Hamiltonian $H_{\text{eff}} = H_0 + H_{\text{e-ph}}$ of the system ought to be mapped to the interval $[-1, 1]$. This is accomplished by rescaling this Hamiltonian, i.e., by introducing

$$\tilde{H} = (1-\varepsilon)\frac{2}{\mathcal{E}_{\max} - \mathcal{E}_{\min}}\left(H_{\text{eff}} - \frac{\mathcal{E}_{\max} + \mathcal{E}_{\min}}{2}\mathbb{1}\right), \tag{C5}$$

where $\mathcal{E}_{\max}$ and $\mathcal{E}_{\min}$ denote the largest and smallest eigenvalues of H_{eff}, respectively; those two eigenvalues can be obtained using the Lanczos algorithm [80]. At the same time, the parameter ε is introduced to avoid stability problems at the boundaries of the spectrum; we hereafter set $\varepsilon = 0.01$.

By inserting the last definition of $\tilde{H}$ into the general expression for the spectral function [cf. Eq. (5)], one arrives at

$$A(k,\omega) = \frac{2\hbar(1-\varepsilon)}{\mathcal{E}_{\max} - \mathcal{E}_{\min}}\sum_j \left|\langle\psi_k^{(j)}| c_k^\dagger |0\rangle\right|^2 \delta\left(\tilde{\omega} - \tilde{E}_k^{(j)}\right), \tag{C6}$$

where $\tilde{E}_k^{(j)}$ represent the eigenvalues of $\tilde{H}$, and the rescaled frequency, given by

$$\tilde{\omega} = \frac{2(1-\varepsilon)}{\mathcal{E}_{\max} - \mathcal{E}_{\min}}\left(\hbar\omega - \frac{\mathcal{E}_{\max} + \mathcal{E}_{\min}}{2}\right), \tag{C7}$$

complies with the rescaling of the Hamiltonian in Eq. (C5).

It is worthwhile to recast Eq. (C6) more succinctly as

$$A(k,\omega) = \frac{2\hbar(1-\varepsilon)}{\mathcal{E}_{\max} - \mathcal{E}_{\min}} f_k(\tilde{\omega}), \tag{C8}$$

where the function $f_k(x)$ is defined as

$$f_k(x) \equiv \langle 0| c_k \delta(x - \tilde{H}) c_k^\dagger |0\rangle . \tag{C9}$$

The delta distribution $\delta(x - \tilde{H})$ can now be expanded in terms of Chebyshev polynomials $T_n(x)$ and approximated by $f_k^{(N_C)}(x)$ with a large order N_C, as introduced in Eq. (C3). For the sake of obtaining a good resolution, we evaluate as many as $N_C = 10^5$ moments.

The Chebyshev moments can be derived based on the general definition in Eq. (C2), which leads to the sought-after expression for the Chebyshev moments:

$$\mu_k^{(n)} = \langle 0| c_k T_n(\tilde{H}) c_k^\dagger |0\rangle \quad (n = 0, \ldots, N_C - 1). \tag{C10}$$

To compute these moments efficiently, it is pertinent to make use of the recurrence relation for Chebyshev polynomials of the first kind [77]:

$$T_{n+1}(x) = 2xT_n(x) - T_{n-1}(x) \quad (n \geqslant 1). \tag{C11}$$

Motivated by this recurrence relation, we define the states $|\alpha_k^{(0)}\rangle \equiv c_k^\dagger |0\rangle$ and $|\alpha_k^{(1)}\rangle \equiv \tilde{H}|\alpha_k^{(0)}\rangle$, as well as

$$\left|\alpha_k^{(n+1)}\right\rangle \equiv 2\tilde{H}\left|\alpha_k^{(n)}\right\rangle - \left|\alpha_k^{(n-1)}\right\rangle, \tag{C12}$$

for $n = 2, \ldots, N_C - 1$.

It is worthwhile noting that the states in Eq. (C12) automatically occur when applying the recurrence relation (C11) to Eq. (C10). Moreover, they render the computation of the Chebyshev moments rather straightforward. Namely, starting from $\mu_k^{(0)} = 1$ and $\mu_k^{(1)} = \langle\alpha_k^{(1)}|\alpha_k^{(0)}\rangle$, one arrives at the following expressions:

$$\begin{aligned}\mu_k^{(2n)} &= 2\left\langle\alpha_k^{(n)}\middle|\alpha_k^{(n)}\right\rangle - \mu_k^{(0)},\\ \mu_k^{(2n+1)} &= 2\left\langle\alpha_k^{(n+1)}\middle|\alpha_k^{(n)}\right\rangle - \mu_k^{(1)}.\end{aligned} \tag{C13}$$

This procedure allows a resource-friendly computation, as the states $|\alpha_k^{(n)}\rangle$, being subject to Eq. (C12), can successively be overwritten. As a matter of fact, only three states $|\alpha_k^{(n)}\rangle$ have to be stored at each computational step.

It is pertinent at this point to comment on the final steps in the evaluation of the spectral function. In the interest of numerical efficiency, it is worthwhile to consider the following special choice of values for the rescaled frequency:

$$\tilde{\omega}_j = \cos\left[\frac{\pi}{N_C}\left(j + \frac{1}{2}\right)\right] \quad (j = 0, \ldots, N_C - 1). \tag{C14}$$

By inserting this last expression for $\tilde{\omega}_j$ into Eq. (C3) and making use of the identity $T_n(\cos y) = \cos(ny)$ for $y \in [-1, 1]$, we

obtain the following result for $f_k^{(N_C)}(\tilde{\omega}_j)$:

$$f_k^{(N_C)}(\tilde{\omega}_j) = \frac{1}{\pi \sin\left[\frac{\pi}{N_C}\left(j+\frac{1}{2}\right)\right]} \times \left\{\mu_k^{(0)} g_0 + 2\sum_{n=1}^{N_C-1} \mu_k^{(n)} g_n \cos\left[n\frac{\pi}{N_C}\left(j+\frac{1}{2}\right)\right]\right\}. \tag{C15}$$

It is worthwhile to mention that this last expression gives rise to a discrete Fourier transformation that can be carried out with a modest computational effort—more precisely, with $O(N_C \log_2 N_C)$ operations—using the well-known fast Fourier transformation (FFT) algorithm [81]. This represents the key benefit of using Chebyshev polynomials of the first kind in the problem at hand.

Having carried out the computation of $f_k^{(N_C)}(\tilde{\omega}_j)$, it remains to insert the obtained result into the approximated form

$$A(k,\omega_j) \approx \frac{2\hbar(1-\varepsilon)}{\mathcal{E}_{\max}-\mathcal{E}_{\min}} f_k^{(N_C)}(\tilde{\omega}_j) \tag{C16}$$

of Eq. (C8) and rescale the energy values as

$$\omega_j = \frac{\mathcal{E}_{\max}-\mathcal{E}_{\min}}{2\hbar(1-\varepsilon)}\tilde{\omega}_j + \frac{\mathcal{E}_{\max}+\mathcal{E}_{\min}}{2\hbar}, \tag{C17}$$

which follows directly from Eq. (C7).

[1] I. M. Georgescu, S. Ashhab, and F. Nori, Rev. Mod. Phys. **86**, 153 (2014).
[2] M. Hohenadler, M. Aichhorn, L. Pollet, and S. Schmidt, Phys. Rev. A **85**, 013810 (2012).
[3] A. A. Gangat, I. P. McCulloch, and G. J. Milburn, Phys. Rev. X **3**, 031009 (2013).
[4] E. Kapit, Phys. Rev. A **87**, 062336 (2013).
[5] F. Yang, L. Henriet, A. Soret, and K. Le Hur, Phys. Rev. B **98**, 035431 (2018).
[6] U. L. Heras, A. Mezzacapo, L. Lamata, S. Filipp, A. Wallraff, and E. Solano, Phys. Rev. Lett. **112**, 200501 (2014).
[7] D. J. Egger and F. K. Wilhelm, Phys. Rev. Lett. **111**, 163601 (2013).
[8] J. Leppäkangas, J. Braumüller, M. Hauck, J.-M. Reiner, I. Schwenk, S. Zanker, L. Fritz, A. V. Ustinov, M. Weides, and M. Marthaler, Phys. Rev. A **97**, 052321 (2018).
[9] I. Bloch, J. Dalibard, and W. Zwerger, Rev. Mod. Phys. **80**, 885 (2008).
[10] For an up-to-date review of Rydberg-atom based platforms, see, e.g., M. Morgado and S. Whitlock, AVS Quantum Sci. **3**, 023501 (2021).
[11] For a recent review of trapped-ion based platforms, see, e.g., C. D. Bruzewicz, J. Chiaverini, R. McConnell, and J. M. Sage, Appl. Phys. Rev. **6**, 021314 (2019).
[12] For a review, see B. Gadway and B. Yan, J. Phys. B **49**, 152002 (2016).
[13] G. S. Paraoanu, J. Low. Temp. Phys. **175**, 633 (2014).
[14] For a recent review on superconducting qubits, see G. Wendin, Rep. Prog. Phys. **80**, 106001 (2017).
[15] J. Koch, T. M. Yu, J. Gambetta, A. A. Houck, D. I. Schuster, J. Majer, A. Blais, M. H. Devoret, S. M. Girvin, and R. J. Schoelkopf, Phys. Rev. A **76**, 042319 (2007).
[16] A. Wallraff, D. I. Schuster, A. Blais, L. Frunzio, R.-S. Huang, J. Majer, S. Kumar, S. M. Girvin, and R. J. Schoelkopf, Nature (London) **431**, 162 (2004).
[17] S. M. Girvin, in *Quantum Machines Measurement and Control of Engineered Quantum Systems*, edited by M. Devoret, Lecture Notes of the Les Houches Summer School, Vol. 96 (Oxford University Press, Oxford, UK, 2014).
[18] For an up-to-date review, see A. Blais, A. L. Grimsmo, S. M. Girvin, and A. Wallraff, Rev. Mod. Phys. **93**, 025005 (2021).
[19] P. A. Volkov and M. V. Fistul, Phys. Rev. B **89**, 054507 (2014).
[20] M. V. Fistul, O. Neyenhuys, A. B. Bocaz, M. Lisitskiy, and I. M. Eremin, Phys. Rev. B **105**, 104516 (2022).
[21] D. Hendry and A. E. Feiguin, Phys. Rev. B **100**, 245123 (2019).
[22] M. L. Baez, M. Goihl, J. Haferkamp, J. Bermejo-Vega, M. Gluza, and J. Eisert, Proc. Natl. Acad. Sci. (USA) **117**, 26123 (2020).
[23] V. M. Stojanović, M. Vanević, E. Demler, and L. Tian, Phys. Rev. B **89**, 144508 (2014).
[24] V. M. Stojanović and I. Salom, Phys. Rev. B **99**, 134308 (2019).
[25] For an introduction, see U. Vool and M. Devoret, Int. J. Circ. Theor. Appl. **45**, 897 (2017).
[26] For a review, see X. Gu, A. Frisk Kockum, A. Miranowicz, Y.-X. Liu, and F. Nori, Phys. Rep. **718-719**, 1 (2017).
[27] For an introduction into SC quantum devices, see Y. Y. Gao, M. A. Rol, S. Touzard, and C. Wang, PRX Quantum **2**, 040202 (2021).
[28] For a systematic introduction into SC circuits, see S. E. Rasmussen, K. S. Christensen, S. P. Pedersen, L. B. Kristensen, T. Bækkegaard, N. J. S. Loft, and N. T. Zinner, PRX Quantum **2**, 040204 (2021).
[29] For a comprehensive review, see P. Krantz, M. Kjaergaard, F. Yan, T. P. Orlando, S. Gustavsson, and W. D. Oliver, Appl. Phys. Rev. **6**, 021318 (2019).
[30] M. C. Cross and D. S. Fisher, Phys. Rev. B **19**, 402 (1979).
[31] W. Barford and R. J. Bursill, Phys. Rev. Lett. **95**, 137207 (2005).
[32] See, e.g., D. Foerster, *Hydrodynamic Fluctuations, Broken Symmetry, and Correlation Functions* (Addison Wesley, Reading, MA, 1983).
[33] For an extensive review, see A. Weiße, G. Wellein, A. Alvermann, and H. Fehske, Rev. Mod. Phys. **78**, 275 (2006).
[34] R. N. Silver and H. Röder, Phys. Rev. E **56**, 4822 (1997).
[35] A. Alvermann and H. Fehske, Phys. Rev. B **77**, 045125 (2008).
[36] G. Schubert, G. Wellein, A. Weisse, A. Alvermann, and H. Fehske, Phys. Rev. B **72**, 104304 (2005).
[37] See, e.g., J. E. Sobczyk and A. Roggero, Phys. Rev. E **105**, 055310 (2022).
[38] M. Knap, A. Kantian, T. Giamarchi, I. Bloch, M. D. Lukin, and E. Demler, Phys. Rev. Lett. **111**, 147205 (2013).
[39] N. F. Ramsey, Phys. Rev. **78**, 695 (1950).
[40] C. Rigetti, J. M. Gambetta, S. Poletto, B. L. T. Plourde, J. M. Chow, A. D. Córcoles, J. A. Smolin, S. T. Merkel, J. R. Rozen,

G. A. Keefe, M. B. Rothwell, M. B. Ketchen, and M. Steffen, Phys. Rev. B **86**, 100506(R) (2012).
[41] T. Holstein, Ann. Phys. **8**, 343 (1959).
[42] E. Jeckelmann and S. R. White, Phys. Rev. B **57**, 6376 (1998).
[43] J. Bonča, S. A. Trugman, and I. Batistić, Phys. Rev. B **60**, 1633 (1999).
[44] L.-C. Ku, S. A. Trugman, and J. Bonča, Phys. Rev. B **65**, 174306 (2002).
[45] V. M. Stojanović, P. A. Bobbert, and M. A. J. Michels, Phys. Rev. B **69**, 144302 (2004).
[46] C. Slezak, A. Macridin, G. A. Sawatzky, M. Jarrell, and T. A. Maier, Phys. Rev. B **73**, 205122 (2006).
[47] K. Hannewald, V. M. Stojanović, J. M. T. Schellekens, P. A. Bobbert, G. Kresse, and J. Hafner, Phys. Rev. B **69**, 075211 (2004).
[48] K. Hannewald, V. M. Stojanović, and P. A. Bobbert, J. Phys.: Condens. Matter **16**, 2023 (2004).
[49] O. Rösch, O. Gunnarsson, X. J. Zhou, T. Yoshida, T. Sasagawa, A. Fujimori, Z. Hussain, Z.-X. Shen, and S. Uchida, Phys. Rev. Lett. **95**, 227002 (2005).
[50] N. Vukmirović, V. M. Stojanović, and M. Vanević, Phys. Rev. B **81**, 041408(R) (2010).
[51] V. M. Stojanović, N. Vukmirović, and C. Bruder, Phys. Rev. B **82**, 165410 (2010).
[52] S. Ciuchi and S. Fratini, Phys. Rev. Lett. **106**, 166403 (2011).
[53] N. Vukmirović, C. Bruder, and V. M. Stojanović, Phys. Rev. Lett. **109**, 126407 (2012).
[54] I. A. Makarov, E. I. Shneyder, P. A. Kozlov, and S. G. Ovchinnikov, Phys. Rev. B **92**, 155143 (2015).
[55] E. I. Shneyder, S. V. Nikolaev, M. V. Zotova, R. A. Kaldin, and S. G. Ovchinnikov, Phys. Rev. B **101**, 235114 (2020).
[56] E. I. Shneyder, M. V. Zotova, S. V. Nikolaev, and S. G. Ovchinnikov, Phys. Rev. B **104**, 155153 (2021).
[57] V. M. Stojanović and M. Vanević, Phys. Rev. B **78**, 214301 (2008).
[58] B. Gerlach and H. Löwen, Phys. Rev. B **35**, 4291 (1987); **35**, 4297 (1987).
[59] V. M. Stojanović, Phys. Rev. B **101**, 134301 (2020).
[60] G. Roósz and K. Held, Phys. Rev. B **106**, 195404 (2022).
[61] V. M. Stojanović, T. Shi, C. Bruder, and J. I. Cirac, Phys. Rev. Lett. **109**, 250501 (2012).
[62] F. Herrera and R. V. Krems, Phys. Rev. A **84**, 051401(R) (2011); F. Herrera, K. W. Madison, R. V. Krems, and M. Berciu, Phys. Rev. Lett. **110**, 223002 (2013).
[63] F. Mei, V. M. Stojanović, I. Siddiqi, and L. Tian, Phys. Rev. B **88**, 224502 (2013).
[64] A. Peres, Phys. Rev. A **32**, 3266 (1985).
[65] M. Heyl, Rep. Prog. Phys. **81**, 054001 (2018).
[66] See, e.g., P. Coleman, *Introduction to Many-Body Physics* (Cambridge University Press, Cambridge, UK, 2015).
[67] For another example of superconducting coupler, see, e.g., H. Lagemann, D. Willsch, M. Willsch, F. Jin, H. De Raedt, and K. Michielsen, Phys. Rev. A **106**, 022615 (2022).
[68] V. M. Stojanović, Phys. Rev. Lett. **124**, 190504 (2020).
[69] T. Haase, G. Alber, and V. M. Stojanović, Phys. Rev. Res. **4**, 033087 (2022).
[70] S. Engelsberg and J. R. Schrieffer, Phys. Rev. **131**, 993 (1963).
[71] H. Fehske, A. Alvermann, M. Hohenadler, and G. Wellein, in Proc. Int. School of Physics "Enrico Fermi," Course CLXI, *Polarons in Bulk Materials and Systems with Reduced Dimensionality*, edited by G. Iadonisi, J. Ranninger, and G. de Filippis (IOS Press, Amsterdam, 2006), pp. 285–296.
[72] F. Dorfner, L. Vidmar, C. Brockt, E. Jeckelmann, and F. Heidrich-Meisner, Phys. Rev. B **91**, 104302 (2015).
[73] Z. Huang, A. D Somoza, C. Peng, J. Huang, M. Bo, C. Yao, J. Li, and G. Long, New J. Phys. **23**, 123020 (2021).
[74] V. M. Stojanović, Phys. Rev. A **103**, 022410 (2021).
[75] T. Holstein and H. Primakoff, Phys. Rev. **58**, 1098 (1940).
[76] T. J. Rivlin, *An Introduction to the Approximation of Functions*, Blaisdell Books in Numerical Analysis and Computer Science (Dover Publications, New York, 1981).
[77] See, e.g., H. Shima and T. Nakayama, *Higher Mathematics for Physics and Engineering* (Springer-Verlag, Berlin, 2010).
[78] D. Jackson, Trans. Am. Math. Soc. **13**, 491 (1912).
[79] R. N. Silver, H. Röder, A. F. Voter, and D. J. Kress, J. Comput. Phys. **124**, 115 (1996).
[80] J. K. Cullum and R. A. Willoughby, *Lanczos Algorithms for Large Symmetric Eigenvalue Computations* (Birkhäuser, Boston, 1985).
[81] W. H. Press, S. A. Teukolsky, W. T. Vetterling, and B. P. Flannery, *Numerical Recipes in C: The Art of Scientific Computing* (Cambridge University Press, Cambridge, 1999).